AGU PUBLICATIONS

Geophysical Research Letters

RESEARCH LETTER
10.1002/2015GL065925

Key Points:
- First climatology of North African dust emission mass linked with Harmattan surges (HSs)
- One third of total emission linked to HSs annually and spatially averaged
- Regionally up to 80% of springtime maximum in emission mass is associated with HSs

Supporting Information:
- Supporting Information S1

Correspondence to:
S. Fiedler,
stephanie.fiedler@mpimet.mpg.de

Citation:
Fiedler, S., M. L. Kaplan, and P. Knippertz (2015), The importance of Harmattan surges for the emission of North African dust aerosol, *Geophys. Res. Lett.*, *42*, 9495–9504, doi:10.1002/2015GL065925.

Received 26 AUG 2015
Accepted 14 OCT 2015
Accepted article online 19 OCT 2015
Published online 7 NOV 2015

The importance of Harmattan surges for the emission of North African dust aerosol

S. Fiedler[1,2], M. L. Kaplan[3], and P. Knippertz[4]

[1]Max Planck Institute for Meteorology, Hamburg, Germany, [2]Formerly at Institute of Meteorology and Climate Research, Karlsruhe Institute of Technology, Karlsruhe, Germany, [3]Division of Atmospheric Science, Desert Research Institute, Reno, Nevada, USA, [4]Institute of Meteorology and Climate Research, Karlsruhe Institute of Technology, Karlsruhe, Germany

Abstract Dust aerosol is important in the Earth system, but the relative impact of meteorological mechanisms on North African dust emission remains unclear. This study presents the first climatology of dust emission amounts associated with Harmattan surges (HSs), characterized by postfrontal strengthening of near-surface winds. A new automated identification uses their strong isallobaric winds as an indicator for HSs in 32 years of ERA-Interim reanalysis. Their impact on dust aerosol emission is estimated by combining the identified events with derived dust emissions. The estimate highlights that about one third of the total emission mass is associated with HSs. Spring shows the largest associated emissions of 30–50% of the monthly totals consistent with the largest number and duration of HSs. Regional emission contributions of up to 80% in the north coincide with the overall largest emission maxima in spring. The importance of HSs for dust emission implies that aerosol-climate models need to accurately represent synoptic-scale storms.

1. Introduction

One of the largest uncertainties in understanding the Earth system is currently associated with aerosol. Mineral dust constitutes the largest fraction of aerosol mass in the troposphere and has a multitude of effects. These include effects on (1) the atmospheric transfer of radiation [e.g., *Tegen and Lacis*, 1996; *Haywood et al.*, 2005; *Allan et al.*, 2011], (2) cloud properties and precipitation [e.g., *Rosenfeld et al.*, 2001; *Lohmann and Diehl*, 2006; *Min et al.*, 2009; *Karydis et al.*, 2011; *Shi et al.*, 2014], (3) surface albedo and ecosystems [e.g., *Krinner et al.*, 2006; *Carslaw et al.*, 2010; *Field et al.*, 2010], and (4) air quality and human health [e.g., *Ozer et al.*, 2007; *De Longueville et al.*, 2010].

Despite the importance of dust aerosol, climate and Earth system models have large uncertainties in dust emission [e.g., *Huneeus et al.*, 2011; *Evan et al.*, 2014; *van Noije et al.*, 2014]. Improving dust simulations is difficult due to the scarcity of ground-based observations in remote desert regions. A key uncertainty in dust emission modeling is the near-surface wind speed [e.g., *Timmreck and Schulz*, 2004], so that evaluating processes that drive these winds is a promising approach for model improvements. Different atmospheric processes are known for generating dust-emitting winds in North Africa [e.g., *Knippertz and Todd*, 2012], the largest and most active dust source on Earth [e.g., *Prospero et al.*, 2002]. Recently, the assessment of their climatological importance has been started through identifying associated emission amounts [*Fiedler et al.*, 2013, 2014; *Heinold et al.*, 2013]. The results highlight nocturnal low-level jets (NLLJs) and convective cold pools as dust-emitting mechanisms with different seasonal and regional importance [*Fiedler et al.*, 2013; *Heinold et al.*, 2013], but these do not explain the overall largest emission maximum along the northern fringes of the Sahara in winter and spring. Here mobile and long-lived cyclones occur but do not coincide with the majority of these emissions [*Fiedler et al.*, 2014]. It remains therefore unclear what process causes that emission maximum.

The season and region point to a possible relevance of Harmattan surges (HSs). HSs manifest themselves as postfrontal strengthening of near-surface winds accompanied by a band of strong isallobaric ageostrophic wind (IW) during an extratropical cold-air intrusion [*Knippertz and Fink*, 2006]. Different regions are known for their occurrence, typically in the lee of mountains [e.g., *Garreaud*, 2001; *Knippertz and Fink*, 2006; *Kaplan et al.*, 2011]. HSs are associated with an upper level trough, schematically depicted in Figure 1 for North Africa. These are mostly positively tilted and present during 20% of the time in winter [*Fröhlich and Knippertz*, 2008]. Closer to the surface, HSs take the form of a trailing front typically to the west of an eastward moving cyclone (Figure 1a). An impressive HS occurred between 1 and 6 March 2004 [*Knippertz and Fink*, 2006; *Li et al.*, 2007;

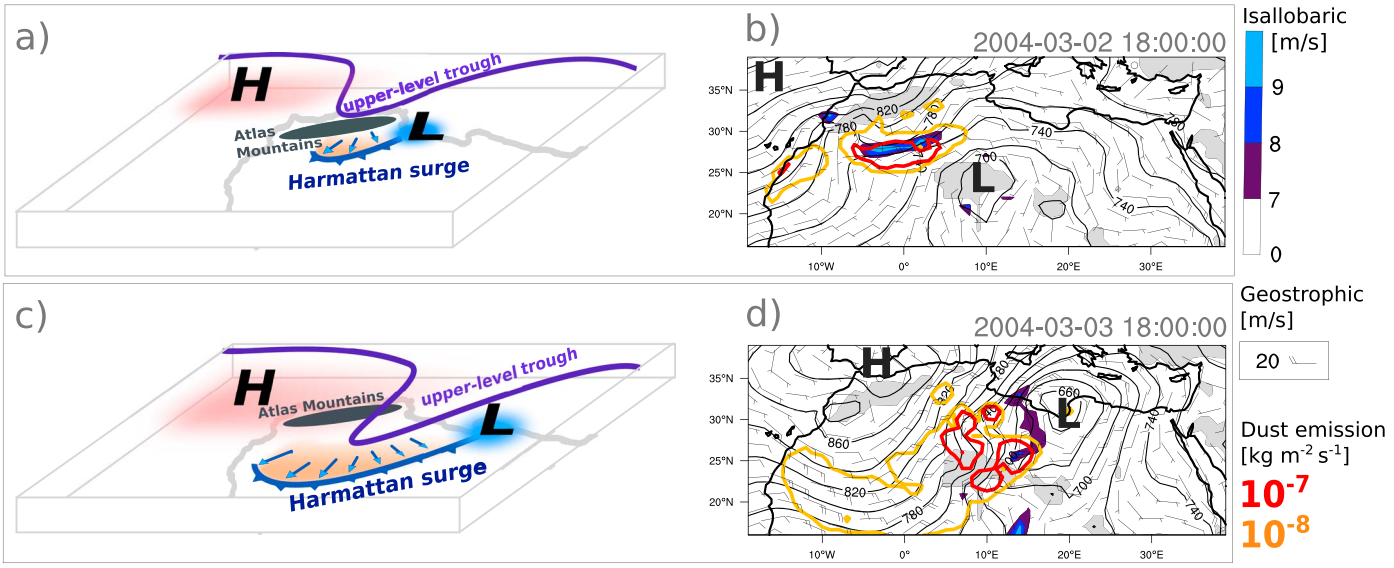

Figure 1. Schematic illustration of (a, c) a Harmattan surge and (b, d) an example from March 2004. Figures 1a and 1b show initiation of HS with strong isallobaric and geostrophic winds to the south of the Atlas Mountains. Figures 1c and 1d show subsequent long-trailing front and continental-scale dust emission. (b, d) Shown are geopotential height (contours), geostrophic winds (wind barbs), isallobaric winds (shaded) at 925 hPa, and total dust emission exceeding 10^{-8} kg m^{-2} s^{-1} (yellow) and 10^{-7} kg m^{-2} s^{-1} (red) during the last 3 h from ERA-Interim data.

Min et al., 2009; *Shao et al.*, 2010; *Mangold et al.*, 2011; *Gläser et al.*, 2012], shown in Figure 1b. The equatorward advection of the extratropical air rapidly increases the near-surface pressure, which causes strong postfrontal near-surface winds. These mobilize dust that marks the front (Figure 1c). The decreasing Coriolis parameter toward the equator prevents a quick adjustment of the atmospheric flow, in contrast to higher latitudes, where the Coriolis force helps to limit the spatial impact of similar storms [*Kaplan et al.*, 2011, 2013; *Lewis et al.*, 2011]. In consequence, HSs propagate over long distances, activating dust sources across the entire North Africa (Figure 1d). The southward advection, e.g., indicated by the typical pressure pattern of HSs in *Klose et al.* [2010], and trans-Atlantic transport [e.g., *Shao et al.*, 2010] of dust from HSs point to their wide influence. Despite their impact, a climatology of their occurrence and associated emission mass is missing.

In the present article HSs are identified in reanalysis over 32 years with a new automated detection. The associated dust emission amount is estimated to better understand the relative importance of HSs compared to other mechanisms. The article is organized as follows. First, the HS detection and the data are described in section 2. Second, a case study is presented as illustration of the method in section 3.1 followed by the mean annual cycle of HSs and their interannual variability (sections 3.2 and 3.3). Section 4 discusses the implications of HSs with respect to other processes, and section 5 presents conclusions.

2. Method

2.1. Model Data

This study makes use of ERA-Interim reanalysis and forecasts from the European Centre for Medium-Range Weather Forecasts [*Dee et al.*, 2011]. Meteorological fields from the 6-hourly reanalysis with a horizontal resolution of 1° are used for the automated detection of HSs. ERA-Interim does not provide dust emission which is therefore calculated with the model by *Tegen et al.* [2002]. The dust emission model is run with instantaneous near-surface winds and soil moisture from 3-hourly ERA-Interim forecasts, which sufficiently capture subdaily variability [*Fiedler et al.*, 2013]. These forecasts are initialized at 00 and 12 UTC with lead times of up to 12 h and simulate similar winds like the reanalysis product [*Fiedler et al.*, 2013]. The setup of the dust emission model follows previous studies [*Fiedler et al.*, 2013, 2014; *Heinold et al.*, 2013]. The modeled dust emissions and winds have been evaluated with available observations [*Fiedler et al.*, 2013, 2014] and intercompared with different models [*Fiedler et al.*, 2015; *Evan et al.*, 2015]. A summary of these evaluations and further observational evidence is provided in the supporting information.

2.2. Automated Detection

HSs are defined by rapidly increasing postfrontal winds, typically affecting northwestern Africa initially and large parts of the Sahara thereafter. For their automated identification, IWs [e.g., *Lewis et al.*, 2011] are calculated at 925 hPa, which are strong due to the rapid change in geopotential height in the postfrontal air. The spatial gradient in the IW is approximated by centered differences considering the neighboring grid boxes, while the geopotential height tendency is calculated over the previous 12 h. Using a period of 6 h gives rather noisy IWs and 24 h misses some peak intensities, such that 12 h has been chosen as compromise.

A filter needs to be applied to avoid detections of spurious IW features. Based on sensitivity tests, HSs are successfully identified if the IW exceeds 7 m s^{-1} in at least five grid boxes in the area 25°–38°N and 15°W–30°E (marked in Figure S1a). The detection area is motivated by the initial influence on northern areas due to the equatorward intrusion of extratropical air. Regions where the 925 hPa level lies below the orography are excluded. The threshold of five grid boxes reflects the banded structure of strong IWs on the order of 500 km. Using a larger number eliminates spurious features but delays the HS detection to later stages such that associated emission at early stages would be missed. Consecutive identifications are treated like a single event in the statistical analysis.

Dust emission from all North African sources is associated with an HS up to 36 h after the last detection. This time period is motivated by ongoing emissions at late stages, when slower pressure changes cause below-threshold IWs. The setup with these thresholds is termed M-7 hereafter. In total, four setups are shown as uncertainty measure: IWs exceeding 7 m s^{-1} (7) and 9 m s^{-1} (9) in at least five (M) and nine (L) grid boxes. The sensitivity to these thresholds is discussed with the climatology. Case studies illustrate the utility of the method next.

3. Results

3.1. Case Studies

The widely discussed HS in March 2004 [e.g., *Knippertz and Fink*, 2006] is briefly investigated here and another three cases of variable strength in the supporting information. These HSs are qualitatively reproduced and successfully detected with the data and method used here.

On 2 March 2004, a positively tilted upper level trough at 200 hPa is situated over northwest Africa with a strong subtropical jet streak (Figure S1g). At 925 hPa, high geopotential lies to the west of the trough and a depression is located over the Hoggar Mountains. The rapid pressure increase in the cool air over northwest Africa, indicated by positive tendencies in geopotential height at 200 hPa (Figure S1g), causes above-threshold IWs near the surface (Figure 1a). Strong near-surface winds mobilize dust [*Knippertz and Fink*, 2006] successfully simulated here (Figure 1a). During the following night, the depression over the Hoggar Mountains shifts eastward and the HS propagates in southerly direction leading to more widespread intense emission over West Africa (Figure 1b). As the upper level trough moves eastward during the subsequent days (Figures S1i–S1l), the HS is associated with dust-emitting winds in more southern and eastern parts of the Sahara (Figures S1b–S1f). These emissions cause the dust suspended behind the long-trailing front as seen in satellite observations (Figure S2) [e.g., *Knippertz and Fink*, 2006]. The continental-scale impact of HSs on emissions, like in March 2004 and 2006 (Figures 1b and 1d and S1 and S2), motivates the association of emissions from the entire North Africa. Even though this may be a generous assumption, case studies of detected short-lived events show substantially smaller associated emissions (Figures S3–S5) despite using the same method for assigning emissions. This evidence is further supported by the climatology of HSs shown next.

3.2. Annual Cycle

3.2.1. Number and Duration of HSs

In order to reflect the variety in HS characteristics and the uncertainty in their detection, HS climatologies are shown for different thresholds (Table S1). M-7 events occur 34 times per year, 21 of which are particularly large (L-7) at the time of first detection. M-9 and L-9 surges are less frequent with a total number of 12 and 6, respectively. Most of the events are detected in spring, shown by the annual cycle of the occurrence of HSs in Figure 2a. The overall maximum of seven M-7 events occurs in April, more than half of which are particularly large (L-7) but less than three with strong IWs exceeding 9 m s^{-1} (M-9). L-9 events are even less frequent with one event in the long-term mean for March and April. July and October have the fewest HSs, while winter months are characterized by three to four M-7 events.

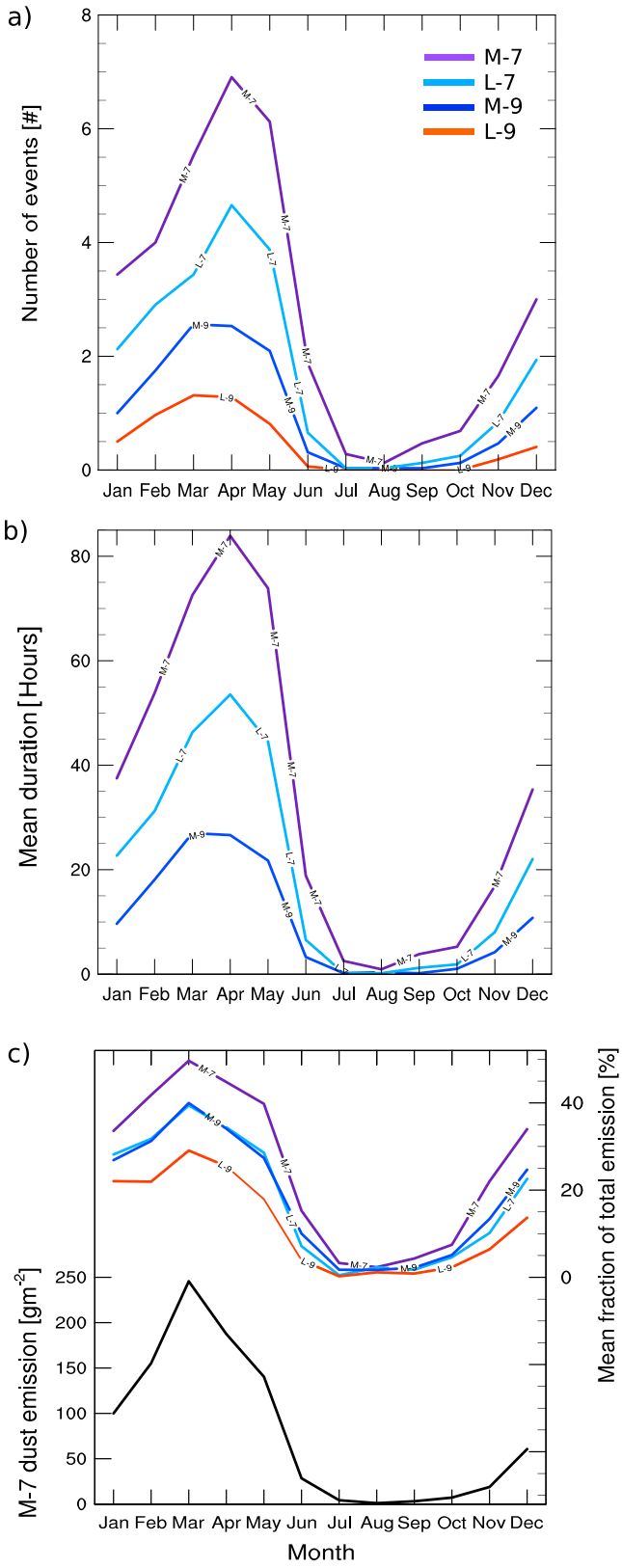

Figure 2. Mean annual cycle of HSs and associated emission. Shown are long-term monthly values of (a) total HS number, (b) mean HS duration, and (c) mean fraction of emission associated with HSs for different thresholds (colors) and total emission associated with M-7 HSs (black) for 1979–2010. L-9 events are too rare for deriving a mean duration.

The number of occurrence does not allow a conclusion on the development and impact on emission of HSs; e.g., a strong HS could be short lived limiting the impact on emission compared to a moderately strong but long-lived case. This motivates an analysis of the duration of HSs. The duration is calculated as the monthly mean time difference between the first and last detection of above-threshold IWs. Figure 2b shows that the annual cycle of the duration is similar to the number of events, suggesting that spring has the most frequent and the longest HSs so that their impact on dust emission is likely to be strongest. The maximum duration in April is 84 h for M-7 surges, 53 h for L-7, and 26 h for M-9. M-7 surges in winter last for 35–55 h which is in good agreement with the mean duration of the influence of upper level troughs [*Fröhlich and Knippertz*, 2008].

3.2.2. Associated Dust Emission

In the annual mean 32% of the total dust emission is associated with M-7 HSs, which corresponds to 133.3 Tg/yr (Table S1). Requiring stronger IWs in a larger area reduces the amount of associated emission to 10% for L-9 events, which is nevertheless substantial in light of only six L-9 HSs in the annual mean. In comparison, mobile cyclones are associated with 4% of the annual emission total but occur almost twice as frequently as L-9 HSs [*Fiedler et al.*, 2014].

Figure 2c shows the annual cycle of the total and relative mass of dust emission associated with HSs. The contribution of M-7 events to emissions shows a clear maximum of 250 g m^{-2} in March which represents 50% of the dust mass in the long-term average across North Africa for this month. Three quarters of these emissions are associated with HSs that were initiated west of 15°E with an emission mean of 190 g m^{-2} in March (not shown). Using more restrictive thresholds reduces the associated emission to a maximum contribution of 30% in March for L-9 events, which is substantial given their rare occurrence (Figure 2a). The maxima in associated emission occurs 1 month earlier than the maximum in the number of M-7 HSs (Figure 2a), reflecting the slightly fewer but more intense HSs and the larger total emission mass in March. The contribution from M-7 HSs decreases to 40% in May followed by a steep decline over the summer months in agreement with few identified events in this season. Dust emission associated with M-7 HSs increases from September onward but remains well below 40% until January. February emissions associated with HSs constitute 42% of the monthly totals corresponding to an amount of 140 g m^{-2} per month. This annual cycle is similar for all thresholds with increasing seasonal differences for larger associated emissions.

The spatial distribution of emission associated with M-7 HSs highlights distinct differences between months, shown in Figure 3. Associated emissions in January are mostly limited to areas north of 25°N with regional contributions of 20–80% to the total emission (Figure 3a), when only few HSs occur over the continent. Areas farther south show an increase in associated emission between February and May, when events are most frequently detected near the Atlas Mountains and over Libya (Figures 3b–3e). Particularly, March shows fractions of 30–80% of the total emission in association with HSs (Figure 3c). This is the time of year when HSs occur frequently and are particularly intense (section 3.2.1). Regional maxima in March are 66% for the rare L-9 events (not shown) underlining the large impact of HSs on emission even when more restrictive criteria are applied. These reductions for L-9 events occur primarily in the northwest (not shown) reflecting the later detection of HSs. June to October are comparably calm with the overall smallest contribution of less than 10% to the emission in August (Figures 3f–3j). November and December show again regional maxima in associated emission with 20–80% for M-7 events, but these are limited to smaller areas than at the beginning of the year (Figures 3k and 3l). These patterns in monthly associated emissions are robust against changes in thresholds for the HS detection.

3.3. Interannual Variability

3.3.1. Number of HSs

Figure 4a shows the time series of the annual total number of HSs, which indicate positive but insignificant trends (Table S1). Circulation anomalies over North Africa can be influenced by the North Atlantic Oscillation (NAO), positive values of which indicate an unusually strong Azores High and thereby an above-average strength of Harmattan winds. However, the correlation coefficients of the anomaly of HS occurrence and the NAO index are low (not shown) for time series of both annual and monthly values as well as April values only, the time of their maximum occurrence frequency. This finding is in agreement with *Fröhlich et al.* [2013] who show low correlations between the NAO index and the occurrence of upper level troughs associated with tropical plumes over North Africa.

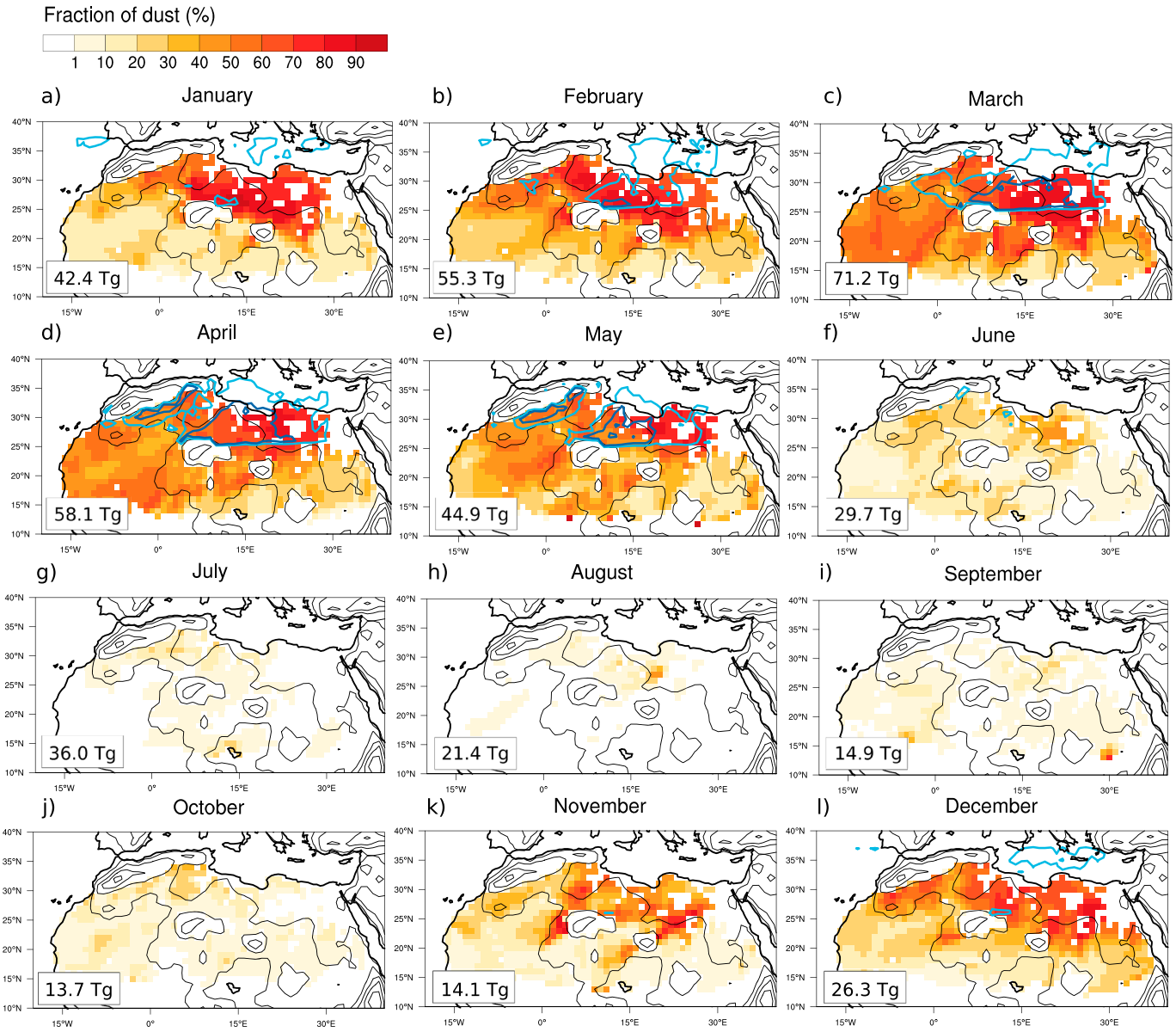

Figure 3. Climatology of dust emission associated with Harmattan surges. Shown are long-term monthly means of fractions of total dust emissions associated with M-7 Harmattan surges (shaded), isolines for IWs above 7 m s^{-1} for 0.5% (light blue) and 1% (dark blue) of the time during a HS, and orography in steps of 400 m. Values are calculated for 1979–2010 and not shown when the 925 hPa isohypse lies below the orography. Amounts in the bottom left corners are long-term means of total North African dust emission per month.

3.3.2. Associated Dust Emission

Figure 4b shows the time series of the annual emission anomalies, calculated as the difference between the annual totals and the long-term average of annual emissions for values associated with HSs and for values for all North African emission. This analysis allows one to categorize individual years relative to the climatological mean. The analysis highlights the overall largest anomaly in 2004 with 110 Tg more emission than usual. Relative to the long-term annual mean of 428 Tg/yr for 1979–2010 [*Fiedler et al.*, 2013], this anomaly corresponds to one quarter of the total emission of North Africa. M-7 HSs are the main contributors to this anomaly with 100 Tg. Likewise, maximum anomalies are found for all other thresholds pointing to the unusually strong impact of HSs in 2004.

In order to assess the impact of individual events, emission anomalies are also calculated as monthly totals minus the long-term average of the same month (not shown). March 2004 has a maximum anomaly of 45 Tg more emission than in the climatological mean. This value corresponds to almost half of the annual anomaly

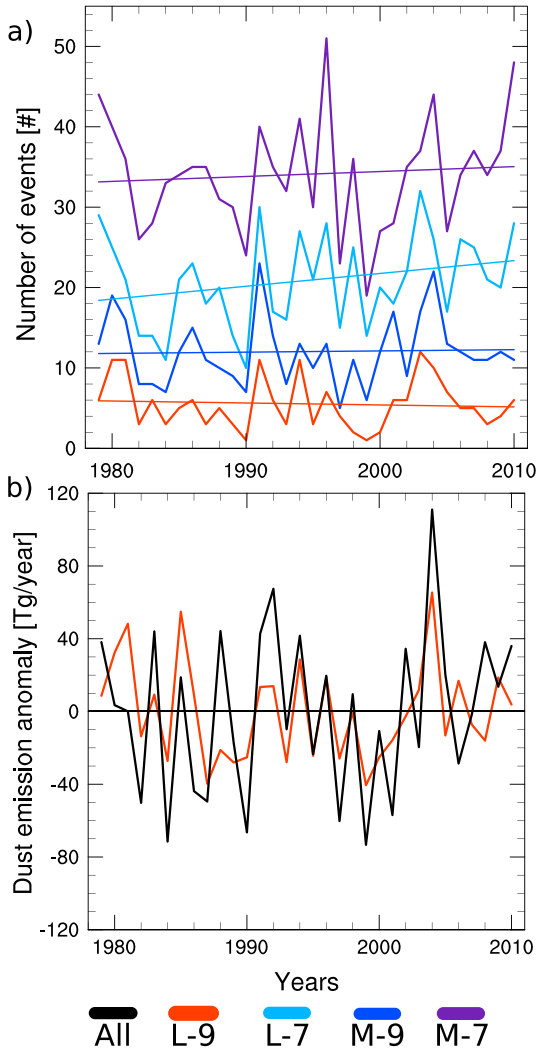

Figure 4. Time series of Harmattan surges. Shown are annual (a) total HS number per year and (b) anomalies in total dust emission (black) and in emission associated with L-9 HSs (orange). Anomalies are calculated as annual total minus the long-term mean. Values are for different thresholds (colors) and based on ERA-Interim. Means and trends are listed in Table S1.

for 2004 (compare Figure 4b). Other HSs show a lower impact on emission; e.g., March 2006 and 2007 are associated with about 15 Tg emission more than usual. These results underline the potentially high but variable impact of HSs on total emission.

4. Discussion

4.1. Uncertainty

The assessment of the importance of HSs for dust aerosol emission from a climatological perspective requires time-dependent and three-dimensional atmospheric data in combination with dust emission fluxes over a period of a few decades. Here ERA-Interim data and the dust emission model by *Tegen et al.* [2002] have been chosen. A similar investigation based on observations alone would not be feasible. The emission data in the present work have been used for identifying other atmospheric processes and their associated dust emission amounts [*Fiedler et al.*, 2013, 2014] and as benchmark for model intercomparison studies [*Fiedler et al.*, 2015; *Evan et al.*, 2015]. In the absence of long-term observations of the dust emission flux, the model performance has been evaluated by using field campaigns, quality-controlled radiosondes, satellite retrievals, and another reanalysis product, the results of which are summarized in the supporting information.

Due to the sparse network of long-term quality-controlled observations in North Africa, a solid validation of near-surface winds and dust aerosol remains difficult. Some progress has been achieved through exploiting available observations [e.g., *Fiedler et al.*, 2013; *Allen and Washington*, 2014], showing differences in winds from reanalysis and observations at single stations. However, the poor spatiotemporal observation coverage over North Africa and local influences on stations are sources for uncertainty, so that local measurements must not be representative for the regional grid box mean in the reanalysis [e.g., *Pinson and Hagedorn*, 2012]. For instance, temporal mismatches of modeled and observed conditions can substantially impact sample statistics [e.g., *Schutgens et al.*, 2015]. Resolving this debate requires more long-term quality-controlled observations from the Sahara.

The emission model in the present work has been developed and optimized for winds in coarse-resolution models [*Tegen et al.*, 2002]. ERA-Interim provides the best near-surface winds among state-of-the-art reanalysis products [*Decker et al.*, 2012; *Largeron et al.*, 2015]. The derived emission shows the same seasonal pattern like another reanalysis wind data set, but the derived mass from ERA-Interim agrees better with other models [*Fiedler et al.*, 2014]. The performance of ERA-Interim is measured at synoptic scales [*Dee et al.*, 2011]. A misrepresentation of HSs therefore seems unlikely, evidence of which has been provided through case studies in the supporting information.

4.2. Embedded Processes

A large fraction of the maximum in dust emission during spring has been associated with HSs. Their contribution to the total annual emission with 32% even exceeds the fraction associated with NLLJs of 15% [*Fiedler et al.*, 2013], which is an important mechanism for North African dust mobilization. NLLJs play a comparably small role for emission along the northern fringes of the Sahara with typically 5–10% [*Fiedler et al.*, 2013] in winter and spring. Here HSs play the most important role for emitting dust aerosol with regionally up to 80%. Farther south NLLJs are associated with large emissions of up to 60% during winter and spring. Parts of them could be simultaneously associated with HSs strengthening NLLJs. For instance, dust storms over the Bodélé Depression are often associated with NLLJs [e.g., *Fiedler et al.*, 2013; *Schwanghart and Schuett*, 2008; *Washington and Todd*, 2005]. Observations show their strengthening due to HSs [*Todd et al.*, 2008], but their impact on emissions is limited to the night and midmorning in contrast to HSs that affect emission throughout the day. The additional amplification of near-surface winds through the NLLJ mechanism therefore plays a small role for dust emission during a strong HS.

Dust emission associated with mobile cyclones forming simultaneously with a HS could be interpreted as part of the same synoptic situation. Emissions associated with mobile cyclones are incorporated in the emission estimate for HSs here but are much smaller. *Fiedler et al.* [2014] show that winds within a 10° circle around the center of mobile cyclones mobilize 4% to the total emission amount in the long-term mean. This cyclone climatology could miss weakly defined open systems, a common feature of all automated cyclone detections so that climatologies differ [*Neu et al.*, 2013]. However, the method in *Fiedler et al.* [2014] identifies more cyclones in the Northern Hemisphere than other techniques, and deep cyclones are generally well captured [*Neu et al.*, 2013]. The assignment of emissions to mobile cyclones in *Fiedler et al.* [2014] uses a search radius for dust emission that is twice as large compared to a study identifying winds as an indicator for the storm intensity [*Bengtsson et al.*, 2009]. Moreover, *Hodges et al.* [2011] show that winds at 925 hPa in extratropical cyclones from ERA-Interim lie within the uncertainty of three other current reanalysis. A substantial underestimation of dust emission associated with mobile closed cyclones in *Fiedler et al.* [2014] seems therefore unlikely.

The results suggest that HSs contribute substantially more to the total emission in winter and spring than mobile closed cyclones or the additional amplification through NLLJs. A stringent separation of the contributions of these mechanisms to emissions is, however, not useful for a generic classification, since they can be linked to the same synoptic situation. These interactions underline the overall importance of the synoptic-scale conditions for dust aerosol production in North Africa during winter and spring.

5. Conclusions

This study statistically investigates the occurrence of Harmattan surges (HSs) and their impact on the North African dust emission mass for 1979–2010. With the aid of a new automated detection for HSs applied to ERA-Interim data, the first climatology of dust emission amounts associated with such storms has been produced. The method has been tested with different thresholds and evaluated with case studies. Requiring isallobaric ageostrophic winds of at least 7 m s^{-1} in five grid boxes suggests that HSs primarily occur and last

longest during spring. Their occurrence frequency and duration in winter and summer are consistent with the statistics of upper level troughs [*Fröhlich and Knippertz*, 2008], which are their synoptic-scale driver.

HSs have been associated with 30–50% of the monthly total emissions in spring spatially averaged and up to 80% regionally. This is the time of year with the largest emission over northern Africa, pointing to the strong impact of HSs on dust emission. Compared to the long-term average of HS emissions, March 2004 is unusual and substantially contributes to the overall largest anomaly in annual total emission. Summer shows the least emissions associated with HSs in agreement with their less frequent occurrence and shorter duration.

The large dust emission associated with HSs in winter and spring underlines the importance of an accurate representation of synoptic-scale storms for emission simulations. State-of-the-art models from CMIP5 disagree on dust emission [*Evan et al.*, 2014] as well as the track density and strength of cyclones, raising concern for the credibility of future changes in such storms [*Zappa et al.*, 2013] with implications going beyond dust aerosol. Comparing atmosphere only and coupled simulations suggests that differences in Mediterranean cyclones are caused by the atmospheric model component [*Zappa et al.*, 2013] and linked to a bias in blocking frequency [*Zappa et al.*, 2014a, 2014b]. *Bengtsson et al.* [2009] show a good performance of ECHAM5 for near-surface winds in cyclones north of 25°N compared to ERA-Interim and observations but a decline of the model performance with coarser resolution. The strongest winds in these storms occur in the cool sector [*Bengtsson et al.*, 2009], similar to the much larger HSs over North Africa. In order to evaluate and possibly improve the key processes for dust-emitting winds from HSs in CMIP6 models, the storm dynamic of HSs needs to be better understood. Flow interaction with the Atlas Mountains helped in generating dust-emitting winds during the HS in March 2004, but several open questions remain [*Gläser et al.*, 2012]. Unbalanced processes probably play an important role in the development of HSs [e.g., *Kaplan et al.*, 2013] and will be further analyzed in an accompanying study.

Acknowledgments
This study is funded by the European Research Council through the "Desert storms" project (257543). We thank Bernd Heinold, Kerstin Schepanski, and Ina Tegen for enabling the dust emission calculations with their model and acknowledge the use of ERA-Interim data from the MARS archive (http://www.ecmwf.int/en/what-mars) of the European Centre for Medium-Range Weather Forecasts made accessible by the UK Met Office. We also acknowledge the mission scientists and associated NASA personnel for the production of the observation data used in this research. We would like to thank the Editor and the anonymous reviewers for their comments that helped us to improve the manuscript.

References

Allan, R. P., M. J. Woodage, S. F. Milton, M. E. Brooks, and J. M. Haywood (2011), Examination of long-wave radiative bias in general circulation models over North Africa during May–July, *Q. J. R. Meteorol. Soc.*, *137*(658), 1179–1192.

Allen, C. J. T., and R. Washington (2014), The low-level jet dust emission mechanism in the central Sahara: Observations from Bordj-Badji Mokhtar during the June 2011 Fennec Intensive Observation Period, *J. Geophys. Res. Atmos.*, *119*, 2990–3015, doi:10.1002/2013JD020594.

Bengtsson, L., K. I. Hodges, and N. Keenlyside (2009), Will extratropical storms intensify in a warmer climate?, *J. Clim.*, *22*(9), 2276–2301, doi:10.1175/2008JCLI2678.1.

Carslaw, K. S., O. Boucher, D. V. Spracklen, G. W. Mann, J. G. L. Rae, S. Woodward, and M. Kulmala (2010), A review of natural aerosol interactions and feedbacks within the Earth system, *Atmos. Chem. Phys.*, *10*(4), 1701–1737.

Decker, M., M. A. Brunke, Z. Wang, K. Sakaguchi, X. Zeng, and M. G. Bosilovich (2012), Evaluation of the reanalysis products from GFSC, NCEP, and ECMWF using flux tower observations, *J. Clim.*, *25*, 1916–1944.

De Longueville, F., Y.-C. Hountondji, S. Henry, and P. Ozer (2010), What do we know about effects of desert dust on air quality and human health in West Africa compared to other regions?, *Sci. Total Environ.*, *409*(1), 1–8.

Dee, D. P., et al. (2011), The ERA-Interim reanalysis: Configuration and performance of the data assimilation system, *Q. J. R. Meteorolog. Soc.*, *137*, 553–597.

Evan, A. T., C. Flamant, S. Fiedler, and O. Doherty (2014), An analysis of aeolian dust in climate models, *Geophys. Res. Lett.*, *41*, 5996–6001, doi:10.1002/2014GL060545.

Evan, A. T., S. Fiedler, C. Zhao, L. Menut, K. Schepanski, C. Flamant, and O. Doherty (2015), Derivation of an observation-based map of North African dust emission, *Aeolian Res.*, *16*, 153–162, doi:10.1016/j.aeolia.2015.01.001.

Fiedler, S., K. Schepanski, B. Heinold, P. Knippertz, and I. Tegen (2013), Climatology of nocturnal low-level jets over North Africa and implications for modeling mineral dust emission, *J. Geophys. Res. Atmos.*, *118*, 6100–6121, doi:10.1002/jgrd.50394.

Fiedler, S., K. Schepanski, P. Knippertz, B. Heinold, and I. Tegen (2014), How important are atmospheric depressions and mobile cyclones for emitting mineral dust aerosol in North Africa?, *Atmos. Chem. Phys.*, *14*, 8983–9000, doi:10.5194/acp-14-8983-2014.

Fiedler, S., P. Knippertz, S. Woodward, G. Martin, N. Bellouin, A. Ross, B. Heinold, K. Schepanski, C. Birch, and I. Tegen (2015), A process-based evaluation of dust-emitting winds in the CMIP5 simulation of HadGEM2-ES, *Clim. Dyn.*,1–24, doi:10.1007/s00382-015-2635-9.

Field, J. P., J. Belnap, D. D. Breshears, J. C. Neff, G. S. Okin, J. J. Whicker, T. H. Painter, S. Ravi, M. C. Reheis, and R. L. Reynolds (2010), The ecology of dust, *Front. Ecol. Environ.*, *8*(8), 423–430, doi:10.1890/090050.

Fröhlich, L., and P. Knippertz (2008), Identification and global climatology of upper-level troughs at low latitudes, *Meteorol. Z.*, *17*(5), 565–573, doi:10.1127/0941-2948/2008/0320.

Fröhlich, L., P. Knippertz, A. H. Fink, and E. Hohberger (2013), An objective climatology of tropical plumes, *J. Clim.*, *26*(14), 5044–5060, doi:10.1175/JCLI-D-12-00351.1.

Garreaud, R. D. (2001), Subtropical cold surges: Regional aspects and global distribution, *Int. J. Climatol.*, *21*(10), 1181–1197, doi:10.1002/joc.687.

Gläser, G., P. Knippertz, and B. Heinold (2012), Orographic effects and evaporative cooling along a subtropical cold front: The case of the spectacular Saharan dust outbreak of March 2004, *Mon. Weather Rev.*, *140*(8), 2520–2533, doi:10.1175/MWR-D-11-00315.1.

Haywood, J., R. Allan, I. Culverwell, T. Slingo, S. Milton, J. Edwards, and N. Clerbaux (2005), Can desert dust explain the outgoing longwave radiation anomaly over the Sahara during July 2003?, *J. Geophys. Res.*, *110*, D05105, doi:10.1029/2004JD005232.

Heinold, B., P. Knippertz, J. H. Marsham, S. Fiedler, N. S. Dixon, K. Schepanski, B. Laurent, and I. Tegen (2013), The role of deep convection and nocturnal low-level jets for dust emission in summertime West Africa: Estimates from convection-permitting simulations, *J. Geophys. Res. Atmos.*, *118*, 4385–4400, doi:10.1002/jgrd.50402.

Hodges, K. I., R. W. Lee, and L. Bengtsson (2011), A comparison of extratropical cyclones in recent reanalyses ERA-Interim, NASA MERRA, NCEP CFSR, and JRA-25, *J. Clim.*, *24*, 4888–4906, doi:10.1175/2011JCLI4097.1.
Huneeus, N., et al. (2011), Global dust model intercomparison in AeroCom phase I, *Atmos. Chem. Phys.*, *11*(15), 7781–7816, doi:10.5194/acp-11-7781-2011.
Kaplan, M. L., R. K. Vellore, J. M. Lewis, and M. Young (2011), The role of unbalanced mesoscale circulations in dust storms, *J. Geophys. Res.*, *116*, D23101, doi:10.1029/2011JD016218.
Kaplan, M. L., R. K. Vellore, J. M. Lewis, S. J. Underwood, P. M. Pauley, J. E. Martin, and R. Krishnan (2013), Re-examination of the I-5 dust storm, *J. Geophys. Res. Atmos.*, *118*, 627–642, doi:10.1002/jgrd.50131.
Karydis, V. A., P. Kumar, D. Barahona, I. N. Sokolik, and A. Nenes (2011), On the effect of dust particles on global cloud condensation nuclei and cloud droplet number, *J. Geophys. Res.*, *116*, D23204, doi:10.1029/2011JD016283.
Klose, M., Y. Shao, M. K. Karremann, and A. Fink (2010), Sahel dust zone and synoptic background, *Geophys. Res. Lett.*, *37*, L09802, doi:10.1029/2010GL042816.
Knippertz, P., and A. H. Fink (2006), Synoptic and dynamic aspects of an extreme springtime Saharan dust outbreak, *Q. J. R. Meteorol. Soc.*, *132*(617), 1153–1177, doi:10.1256/qj.05.109.
Knippertz, P., and M. C. Todd (2012), Mineral dust aerosol over the Sahara: Processes of emission and transport, and implifications for modeling, *Rev. Geophys.*, *50*, RG1007, doi:10.1029/2011RG000362.
Krinner, G., O. Boucher, and Y. Balkanski (2006), Ice-free glacial northern Asia due to dust deposition on snow, *Clim. Dyn.*, *27*(6), 613–625.
Largeron, Y., F. Guichard, D. Bouniol, F. Couvreux, L. Kergoat, and B. Marticorena (2015), Can we use surface wind fields from meteorological reanalyses for Sahelian dust emission simulations?, *Geophys. Res. Lett.*, *42*, 2490–2499, doi:10.1002/2014GL062938.
Lewis, J. M., M. L. Kaplan, R. Vellore, R. M. Rabin, J. Hallett, and S. A. Cohn (2011), Dust storm over the Black Rock Desert: Larger-scale dynamic signatures, *J. Geophys. Res.*, *116*, D06113, doi:10.1029/2010JD014784.
Li, J., P. Zhang, T. J. Schmit, J. Schmetz, and W. P. Menzel (2007), Technical note: Quantitative monitoring of a Saharan dust event with SEVIRI on Meteosat-8, *Int. J. Remote Sens.*, *28*(10), 2181–2186, doi:10.1080/01431160600975337.
Lohmann, U., and K. Diehl (2006), Sensitivity studies of the importance of dust ice nuclei for the indirect aerosol effect on stratiform mixed-phase clouds, *J. Atmos. Sci.*, *63*(3), 968–982, doi:10.1175/JAS3662.1.
Mangold, A., et al. (2011), Aerosol analysis and forecast in the European Centre for Medium-Range Weather Forecasts integrated forecast system: 3. Evaluation by means of case studies, *J. Geophys. Res.*, *116*, D03302, doi:10.1029/2010JD014864.
Min, Q.-L., R. Li, B. Lin, E. Joseph, S. Wang, Y. Hu, V. Morris, and F. Chang (2009), Evidence of mineral dust altering cloud microphysics and precipitation, *Atmos. Chem. Phys.*, *9*(9), 3223–3231, doi:10.5194/acp-9-3223-2009.
Neu, U., et al. (2013), IMILAST: A community effort to intercompare extratropical cyclone detection and tracking algorithms, *Bull. Am. Meteorol. Soc.*, *94*(4), 529–547.
Ozer, P., M. Laghdaf, S. Lemine, and J. Gassani (2007), Estimation of air quality degradation due to Saharan dust at Nouakchott, Mauritania, from horizontal visibility data, *Water Air Soil Pollut.*, *178*(1–4), 79–87, doi:10.1007/s11270-006-9152-8.
Pinson, P., and R. Hagedorn (2012), Verification of the ECMWF ensemble forecasts of wind speed against analyses and observations, *Meteorol. Appl.*, *19*(4), 484–500.
Prospero, J. M., P. Ginoux, O. Torres, S. E. Nicholson, and T. E. Gill (2002), Environmental characterization of global sources of atmospheric soil dust identified with the NIMBUS 7 Total Ozone Mapping Spectrometer (TOMS) absorbing aerosol product, *Rev. Geophys.*, *40*(1), 1002, doi:10.1029/2000RG000095.
Rosenfeld, D., Y. Rudich, and R. Lahav (2001), Desert dust suppressing precipitation: A possible desertification feedback loop, *Proc. Natl. Acad. Sci.*, *98*(11), 5975–5980.
Schutgens, N. A. J., D. G. Partridge, and P. Stier (2015), The importance of temporal collocation for the evaluation of aerosol models with observations, *Atmos. Chem. Phys. Discuss.*, *15*(18), 26,191–26,230, doi:10.5194/acpd-15-26191-2015.
Schwanghart, W., and B. Schuett (2008), Meteorological causes of Harmattan dust in West Africa, *Geomorphology*, *95*(3-4), 412–428, doi:10.1016/j.geomorph.2007.07.002.
Shao, Y., A. H. Fink, and M. Klose (2010), Numerical simulation of a continental-scale Saharan dust event, *J. Geophys. Res.*, *115*, D13205, doi:10.1029/2009JD012678.
Shi, J. J., T. Matsui, W.-K. Tao, Q. Tan, C. Peters-Lidard, M. Chin, K. Pickering, N. Guy, S. Lang, and E. M. Kemp (2014), Implementation of an aerosol-cloud-microphysics radiation coupling into the NASA unified WRF: Simulation results for the 6-7 August 2006 AMMA special observing period, *Q. J. R. Meteorol. Soc.*, *140*(684), 2158–2175, doi:10.1002/qj.2286.
Tegen, I., and A. A. Lacis (1996), Modeling of particle size distribution and its influence on the radiative properties of mineral dust aerosol, *J. Geophys. Res.*, *101*(D14), 19,237–19,244.
Tegen, I., S. Harrison, K. Kohfeld, I. Prentice, M. Coe, and M. Heimann (2002), Impact of vegetation and preferential source areas on global dust aerosol: Results from a model study, *J. Geophys. Res.*, *107*(D21), 4576, doi:10.1029/2001JD000963.
Timmreck, C., and M. Schulz (2004), Significant dust simulation differences in nudged and climatological operation mode of the AGCM ECHAM, *J. Geophys. Res.*, *109*, D13202, doi:10.1029/2003JD004381.
Todd, M. C., R. Washington, S. Raghavan, G. Lizcano, and P. Knippertz (2008), Regional model simulations of the Bodele low-level jet of northern Chad during the Bodélé Dust Experiment (BoDEx 2005), *J. Clim.*, *21*(5), 995–1012, doi:10.1175/2007JCLI1766.1.
van Noije, T. P. C., P. Le Sager, A. J. Segers, P. F. J. van Velthoven, M. C. Krol, W. Hazeleger, A. G. Williams, and S. D. Chambers (2014), Simulation of tropospheric chemistry and aerosols with the climate model EC-Earth, *Geosci. Model Dev.*, *7*(5), 2435–2475, doi:10.5194/gmd-7-2435-2014.
Washington, R., and M. Todd (2005), Atmospheric controls on mineral dust emission from the Bodélé Depression, Chad: The role of the low-level jet, *Geophys. Res. Lett.*, *32*, L17701, doi:10.1029/2005GL023597.
Zappa, G., L. C. Shaffrey, and K. I. Hodges (2013), The ability of CMIP5 models to simulate North Atlantic extratropical cyclones, *J. Clim.*, *26*(15), 5379–5396, doi:10.1175/JCLI-D-12-00501.1.
Zappa, G., M. Hawcroft, L. Shaffrey, E. Black, and D. Brayshaw (2014a), Extratropical cyclones and the projected decline of winter Mediterranean precipitation in the CMIP5 models, *Clim. Dyn.*, *45*, 1727–1738, doi:10.1007/s00382-014-2426-8.
Zappa, G., G. Masato, L. Shaffrey, T. Woollings, and K. Hodges (2014b), Linking Northern Hemisphere blocking and storm track biases in the CMIP5 climate models, *Geophys. Res. Let.*, *41*, 135–139, doi:10.1002/2013GL058480.